HHS Public Access

Author manuscript

Cell Rep. Author manuscript; available in PMC 2016 May 31.

Published in final edited form as:

Cell Rep. 2016 May 24; 15(8): 1686–1699. doi:10.1016/j.celrep.2016.04.057.

Impaired mitochondrial fat oxidation induces FGF21 in muscle

Bolormaa Vandanmagsar[1], **Jaycob D. Warfel**[1], **Shawna E. Wicks**[1], **Sujoy Ghosh**[6,7], **J. Michael Salbaum**[2], **David Burk**[3], **Olga S. Dubuisson**[1], **Tamra M. Mendoza**[1], **Jingying Zhang**[4], **Robert C. Noland**[5], and **Randall L. Mynatt**[1,4]

[1]Gene Nutrient Interactions Laboratory, Pennington Biomedical Research Center, Louisiana State University, Baton Rouge, Louisiana

[2]Genomics Core Facility, Pennington Biomedical Research Center, Louisiana State University, Baton Rouge, Louisiana

[3]Cell Biology and Bioimaging Core Facility, Pennington Biomedical Research Center, Louisiana State University, Baton Rouge, Louisiana

[4]Transgenic Core Facility, Pennington Biomedical Research Center, Louisiana State University, Baton Rouge, Louisiana

[5]Skeletal Muscle Metabolism Laboratory, Pennington Biomedical Research Center, Louisiana State University, Baton Rouge, Louisiana

[6]Computational Biology Laboratory, Pennington Biomedical Research Center, Louisiana State University, Baton Rouge, Louisiana

[7]Centre for Computational Biology & Program in Cardiovascular and Metabolic Disorders, Duke-NUS Graduate Medical School, Singapore

SUMMARY

Fatty acids are the primary fuel source for skeletal muscle during most of our daily activities and impaired fatty acid oxidation (FAO) is associated with insulin resistance. We have developed a mouse model of impaired FAO by deleting carnitine palmitoyltransferase-1b specifically in skeletal muscle (*Cpt1b*$^{m-/-}$). *Cpt1b*$^{m-/-}$ mice have increased glucose utilization and are resistant to diet induced obesity. Here we show that inhibition of mitochondrial FAO induces FGF21 expression specifically in skeletal muscle. The induction of FGF21 in Cpt1b-deficient muscle is dependent on AMPK and Akt1 signaling but independent on the stress signaling pathways. FGF21 appears to act in a paracrine manner to increase glucose uptake under low insulin conditions, but does not contribute to the resistance to diet induced obesity.

Corresponding author: Randall L. Mynatt, 6400 Perkins Road, Baton Rouge, LA, 70808, Office: 225-763-3100, Fax: 225-763-0273, ; Email: Randall.Mynatt@pbrc.edu

Author contributions: Data collection and manuscript preparation: BV, JDW, SEW, RCN and RLM. Data analysis: SG and MS. Histology: DB Technical Assistance: OSD, TMM

INTRODUCTION

Fat contributes 90% of the substrate for resting energy expenditure in skeletal muscle and remains the primary fuel during daily activities and low exercise intensities (<40% VO_2max) (Brooks, 1997; Brooks and Mercier, 1994; Dagenais et al., 1976; Kelley et al., 1993). Carnitine palmitoyltransferase-1 (CPT1) is located on the outer mitochondrial membrane and transports long-chain fatty acids into mitochondria for β-oxidation. We created a mouse model of impaired fatty acid oxidation (FAO) by deleting carnitine palmitoyltransferase-1b in skeletal muscle (*Cpt1b*$^{m-/-}$) and reported that inhibition of mitochondrial FAO leads to activation of AMPK and PGC1α, resulting in adaptive metabolic responses in skeletal muscle with increased mitochondrial biogenesis, oxidative capacity, compensatory peroxisomal fat oxidation and amino acid catabolism (Wicks et al., 2015). In addition, despite elevated plasma lipids, and accumulation of both intramyocellular lipids (IMCL) and lipotoxic species, fasting insulin and glucose are lower in *Cpt1b*$^{m-/-}$ mice with enhanced glucose utilization in *Cpt1b*$^{m-/-}$ mice. Here we report what appears to be a local starvation response in which FGF21 is specifically upregulated in skeletal muscle of *Cpt1b*$^{m-/-}$ mice.

FGF21 was identified as a novel member of the FGF family which is highly expressed in liver (Nishimura et al., 2000). FGF21 was subsequently shown to be a potent metabolic regulator of glucose uptake in adipocytes (Kharitonenkov et al, 2005) and is generally thought of as secreted a protein produced by liver in response to starvation (Badman et al., 2007; Inagaki et al., 2007). However, under myopathic conditions resulting from deficiencies in the mitochondrial respiratory chain FGF21 can be secreted from skeletal muscle (Kim et al., 2013b; Tyynismaa et al., 2010). Also the transgenic overexpression of Akt1 (Izumiya et al., 2008), Perilipin-5 (Harris et al., 2015), and UCP1(Keipert et al., 2014; Ost et al., 2016) in skeletal muscle induces FGF21 secretion. The skeletal muscle-specific ablation of autophagy-related 7 (Atg7) leads to an autophagy deficiency and mitochondrial dysfunction and increases FGF21 in muscle (Kim et al., 2013b; Tyynismaa et al., 2010). Also, the skeletal muscle-specific ablation of tuberous sclerosis complex1 (Tsc1) causing activation of mTORC1 induces FGF21 secretion from muscle (Guridi et al., 2015). A common link between these mouse models (except Akt1 overexpression) is metabolic dysfunction, ER stress and activation of Atf4, as a master regulator of the integrative stress response leading to FGF21 induction.

In the present study, we address whether upregulation of FGF21 in skeletal muscle contributes to the enhanced carbohydrate metabolism (improved insulin sensitivity and glucose utilization) in response to inhibition of mitochondrial FAO in *Cpt1b*$^{m-/-}$ mice. We demonstrate that FGF21 can be upregulated by restricting FAO in muscle in an AMPK-Akt1-dependent manner without activation of the integrative stress response. We also determine the role of FGF21 in the overall phenotype of *Cpt1b*$^{m-/-}$ mice using CPT1b and FGF21 double knockout mice (DKO).

RESULTS

Mitochondrial FAO deficiency in muscle induces FGF21

Serum FGF21 levels were significantly higher in both fed and fasted states in *Cpt1b*$^{m-/-}$ mice compared to control mice (Figure 1A). To determine if increased FGF21 in circulation was in part arising from skeletal muscle we examined *Fgf21* gene expression in several tissues. The mRNA expression of *Fgf21* was markedly upregulated in several muscles of *Cpt1b*$^{m-/-}$ mice compared to *Cpt1b*$^{fl/fl}$ mice, without changes in liver or white adipose tissue (Figure 1B).

We next evaluated the effect of muscle-specific upregulation of FGF21 on glucose uptake in skeletal muscle. Gene expression of *Fgfr1* and its spliced variants *Fgfr1b* and *Fgfr1c* were not different in skeletal muscle between *Cpt1b*$^{m-/-}$ and control mice (Figure S1A–1C). However, proteomic (Wicks et al., 2015) and immunoblot analyses of muscle from *Cpt1b*$^{m-/-}$ mice revealed significantly elevated protein expression of β-Klotho in muscle, which is the essential co-receptor for FGF21 (Ogawa et al., 2007) (Figure 1C). Consistent with reports that FGF21 increases glucose uptake via glucose transporter 1 (Kharitonenkov et al., 2005; Mashili et al., 2011), protein expression of Glut1 was markedly increased in muscle of *Cpt1b*$^{m-/-}$ mice compared to controls (Figure 1C).

Primary myotubes from *Cpt1b*$^{m-/-}$ mice have a similar metabolic gene expression profile to those in muscle from *Cpt1b*$^{m-/-}$ mice (Figure S1D–1E). We found significantly increased mRNA expression and protein secretion of FGF21 in primary myotubes derived from *Cpt1b*$^{m-/-}$ mice compared to *Cpt1b*$^{fl/fl}$ mice (Figure 1D and 1E). Basal glucose uptake was significantly elevated in primary myotubes from *Cpt1b*$^{m-/-}$ mice; however, insulin-stimulated glucose uptake was comparable to *Cpt1b*$^{fl/fl}$ mice (Figure 1F). Notably, FGF21 treatment significantly increased glucose uptake in myotubes from both *Cpt1b*$^{m-/-}$ and control mice, suggesting the elevated basal glucose uptake in myotubes from *Cpt1b*$^{m-/-}$ mice is potentially a result from enhanced FGF21 production (Figure 1G).

Insulin sensitivity in *Cpt1b*-deficient muscle is maintained through mTOR-Akt signaling

To determine the underlying molecular mechanisms of increased glucose utilization despite lipotoxity in *Cpt1b*$^{m-/-}$ mice, we first examined mTOR signaling pathway, which senses nutrient and energy levels and integrates upstream and downstream signals including growth factors such as insulin (Wullschleger et al., 2006). Phosphorylation of mTOR at Ser2448, the site associated with mTORC1 activity (Chiang and Abraham, 2005), was significantly decreased in muscle of *Cpt1b*$^{m-/-}$ mice compared to *Cpt1b*$^{fl/fl}$ mice (Figure 2A). Likewise, phosphorylation of P70 isoform of S6K1, the main downstream effector of mTORC1 (Wullschleger et al., 2006), was significantly reduced in skeletal muscle from *Cpt1b*$^{m-/-}$ mice (Figure 2B). Activation of mTORC1 negatively regulates insulin sensitivity via activation of S6K1, which inhibits IRS protein responsiveness to insulin stimulation by directly phosphorylating IRS1 at Ser636/639 (Um et al., 2004; Wullschleger et al., 2006). In *Cpt1b*$^{m-/-}$ skeletal muscle Ser-phosphorylation of IRS1 was significantly decreased, suggesting reduced mTORC1 signaling (Figure 2B). Additionally, Tyr-phosphorylation of IRS1, which facilitates insulin responsiveness (Copps and White, 2012), is significantly

increased in skeletal muscle of *Cpt1b*$^{m-/-}$ mice compared to control mice (Figure S2A). As a consequence of decreased inhibitory action of mTORC1 signaling in *Cpt1b*$^{m-/-}$ muscle in the basal state, we detected significant reductions in basal phosphorylation of both Akt (Ser473) and IR (Tyr1162/1163) in skeletal muscle using multiplex and immunoblot analysis (Figure 2C and S2B). Based upon this evidence we predicted that reduced mTORC1 signaling in the basal state would not only improve basal glucose clearance, but also increase sensitivity of *Cpt1b*$^{m-/-}$ muscle to insulin stimulation. Consistent with this, fasting plasma insulin levels were decreased in *Cpt1b*$^{m-/-}$ mice and remained significantly lower throughout life (Wicks et al., 2015). However, insulin-stimulated phosphorylation of total Akt (Ser473) was comparable between *Cpt1b*$^{m-/-}$ and control mice (Wicks et al., 2015).

The Akt-family includes 3 members:1) *Akt1* is involved in cellular survival pathways (Chen et al., 2001) and gene levels were elevated in muscle of *Cpt1b*$^{m-/-}$ mice; 2) *Akt2* is an important molecule in the insulin signaling pathway (Garofalo et al., 2003), but mRNA expression was not different between genotypes, and 3) *Akt3* was undetectable in skeletal muscle (Figure 2D). Phosphorylation of Akt1 (Ser473) at baseline was not different between genotypes, but insulin-stimulated phosphorylation was significantly greater in skeletal muscle of *Cpt1b*$^{m-/-}$ mice (Figure 2E). Notably, phosphorylation of Akt2 (Ser474) at baseline was significantly decreased in muscle of *Cpt1b*$^{m-/-}$ mice compared to *Cpt1b*$^{fl/fl}$ mice, whereas insulin-stimulated Akt2 phosphorylation was comparable between genotypes (Figure 2F).

To gain further insight into how impaired mitochondrial FAO causes inhibition of mTORC1 signaling, we next examined upstream factors that impact the mTORC1 pathway. TSC1/TSC2 is a critical regulator of mTOR signaling and activation of this complex inhibits mTORC1 (Wullschleger et al., 2006). In contrast, TSC1/TSC2 activates mTORC2, which in turn triggers Akt1 activation (Huang and Manning, 2009). Within the TSC1/TSC2 complex, TSC1 stabilizes TSC2 (Chong-Kopera et al., 2006), which facilitates activation of TSC2 by kinases such as AMPK and Akt that directly phosphorylate TSC2 at Ser-1387 (Inoki et al., 2003) and Thr1462 (Huang and Manning, 2008), respectively. We found significantly elevated phosphorylation of TSC2 at Ser-1387 in muscle of *Cpt1b*$^{m-/-}$ mice, whereas phosphorylation of TSC2 at Thr-1462 was not different. These findings suggest TSC2 activation occurs via AMPK, but not Akt in *Cpt1b*$^{m-/-}$ muscle (Figure 2G). This is consistent with our previous report that mitochondrial FAO deficiency induced a low energy state in skeletal muscle of *Cpt1b*$^{m-/-}$ mice that activated AMPK (Wicks et al., 2015), but extends these findings by suggesting that AMPK stimulates the TSC1/2 complex in *Cpt1b*$^{m-/-}$ mice (Figure 2H). Specifically, these findings suggest that TSC1/2 inhibits mTORC1 signaling resulting in enhanced basal insulin sensitivity, and activates the mTORC2 pathway in *Cpt1b*$^{m-/-}$ mice which increases basal glucose uptake (Figure 2H).

Fgf21 induction in *Cpt1b*-deficient muscle is AMPK- and Akt1-dependent

Within the model shown in Figure 2H we predict AMPK and Akt1 signaling are necessary for induction of FGF21 in skeletal muscle of *Cpt1b*$^{m-/-}$ mice. To test this directly we utilized mouse and human primary muscle cells. In agreement with our mechanistic hypothesis (Figure 2H), expression of *Fgf21* in primary myotubes from *Cpt1b*$^{m-/-}$ mice was

normalized when exposed to either an Akt1-specific inhibitor, A-674563 or an AMPK-inhibitor, Compound C (Figure 3A). To test whether pharmacological inhibition of CPT1b recapitulates effects of genetic inhibition of *Cpt1b*, we exposed primary myotubes from *Cpt1b*$^{fl/fl}$ mice to FA in the presence of the CPT1 inhibitor, Etomoxir. *Fgf21* expression was not induced in the presence of FA alone, but was robustly elevated in myotubes exposed to FA in the presence of Etomoxir in a dose-dependent manner (Figure 3B and S2C).

To study whether the pharmacological inhibition of CPT1 drives FGF21-induction in the insulin-resistant condition, we explored human skeletal muscle myotubes from diabetic-obese subjects. Our previous report demonstrated that these myotubes are insulin-resistant compared to myotubes derived from non-diabetic-lean humans (Vandanmagsar et al., 2014). Treatment with FA induced *FGF21* expression in the presence of Etomoxir in myotubes from both normal-lean and diabetic-obese subjects; however, *FGF21* induction was blunted in myotubes from diabetic-obese subjects (Figure 3C). Notably, exposure to A-674563 and Compound C blunted FA+Etomoxir induction of *FGF21* in myotubes from both groups. (Ferre, 2004). FGF21 is induced by PPARα in liver in response to fasting (Inagaki et al., 2007). However, treatment with inhibitors of PPARα, PPARγ and PPARδ did not affect FA +Etomoxir-induced *FGF21* expression in myotubes from normal-lean subjects (Figure 3D). Collectively, these data indicate involvement of AMPK and Akt1 signaling in FGF21 induction in the mitochondrial FAO deficient condition.

To test whether FGF21 directly imparts beneficial effects on the insulin signaling cascade in the presence of excess FA, we treated human myotubes from normal-lean subjects with rhFGF21 ± FA and determined activity of mTOR and its downstream signaling pathways. In the absence of FA, FGF21 had minimal effects as only phosphorylation of p70S6K was reduced. Alternatively, when FA was present FGF21 was able to reduce phosphorylation of mTor (Ser2448), p70S6K, IRS1 (Ser636/639) and Akt (Ser473) (Figure 3E). Taken together, these data suggest that FGF21 has protective effects on lipid-induced insulin resistance which in turn preserves glucose uptake in muscle in lipotoxic conditions such as in skeletal muscle of *Cpt1b*$^{m-/-}$ mice.

Stress signaling pathways are not activated by mitochondrial fat oxidation deficiency

To determine if other potential signaling pathways leading to induction of FGF21 in skeletal muscle of *Cpt1b*$^{m-/-}$ mice, we evaluated other mechanisms linked to mTOR signaling and FGF21 induction. In *Cpt1b*$^{m-/-}$ mice, systemic and intramyocellular lipids, particularly toxic DAG species are increased (Wicks et al., 2015), thus DAG-signaling could be enhanced. Previous reports have shown that DAG kinases inhibit mTOR activation through repressing Erk1/2 pathways (Gorentla et al., 2011). Erk1/2 directly phosphorylates TSC2, thus negatively regulating mTORC1 signaling (Ma et al., 2005; Wullschleger et al., 2006). Notably, phosphorylation of Erk1/2 was not elevated in skeletal muscle of *Cpt1b*$^{m-/-}$ mice (Figure 4A). In addition, oxidative stress and hypoxia have been linked to mTORC1 activity (Kim et al., 2002; Wouters and Koritzinsky, 2008). Of note, gene expression of oxidative stress (*Nrf2*) and hypoxia (*Hif1α*) markers was not elevated in muscle of *Cpt1b*$^{m-/-}$ mice compared to *Cpt1b*$^{fl/fl}$ mice (Figure 4B–4C). Furthermore, the expression levels of endoplasmic reticulum (ER) stress markers (unspliced *Xbp1u* and spliced *Xbp1s*) were

unchanged in *Cpt1b*$^{m-/-}$ muscle (Figure 4D). Moreover, the ER stress marker *Ddit3* (Haynes and Ron, 2010) expression was significantly decreased in *Cpt1b*$^{m-/-}$ muscle (Figure 4E). In line with these data, Atf4 mRNA and protein expression, as well as *Atf5* mRNA expression in skeletal muscle were similar between *Cpt1b*$^{m-/-}$ and *Cpt1b*$^{fl/fl}$ mice (Figure 4F and S2D).

In addition to the candidate gene approach, we did a comprehensive global expression analysis in gastrocnemius muscle from *Cpt1b*$^{m-/-}$ and control mice. The genes belonging to ER stress, autophagy, and mitophagy pathways were obtained from Gene Ontology, and then compared by pathway enrichment analysis by including these 3 pathways to the standard KEGG pathways. None of these overall pathways were significantly different between *Cpt1b*$^{m-/-}$ and *Cpt1b*$^{fl/fl}$ mice (Figure 4G). In fact, at the gene level, only one gene (*Ppp1r15a*) out of over 200 genes was significantly different between *Cpt1b*$^{m-/-}$ and control mice. Heat maps to show the distribution of expression for genes belonging to these pathways are included in supplementary data (Figure S3–S5). Moreover, uncoupling protein 3 (*Ucp3*) expression was significantly increased in *Cpt1b*$^{m-/-}$ muscle (Figure 4H), suggesting potential beneficial effects, since it has been reported that upregulated expression of UCP3 reduced ER stress (Xu et al., 2015) and ROS production (Nabben et al., 2011). Together, these data indicate that mitochondrial respiratory chain dysfunction and myocellular stress do not appear to be major inducers of FGF21 in *Cpt1b*$^{m-/-}$ muscle and are consistent with our previous report that *Cpt1b*-deficient mitochondria respire efficiently when given substrates other than long chain fatty acids (Wicks et al., 2015). In fact, pathways for oxidative phosphorylation, TCA cycle and overall mitochondrial biogenesis are upregulated in *Cpt1b*$^{m-/-}$ muscle (Wicks et al., 2015).

Loss of FGF21 increases muscle mass, activity, energy expenditure and oxidative capacity but does not alter adiposity in *Cpt1b*$^{m-/-}$ mice

To determine the extent of FGF21's role in the overall phenotype of the *Cpt1b*$^{m-/-}$ mice, we generated double knockout mice, (DKO (*Fgf21*$^{-/-}$ *Cpt1b*$^{m-/-}$) by crossing *Fgf21*$^{-/-}$ mice (Badman et al., 2009; Hotta et al., 2009) with *Cpt1b*$^{m-/-}$ mice. As shown in Figure 5A, there was an intermediate effect on bodyweight in the DKO mice. The DKO mice were significantly heavier than *Cpt1b*$^{m-/-}$ mice but did not reach the bodyweight of control or *Fgf21*$^{-/-}$ mice (Figure 5A). However, there was no difference in fat mass between *Cpt1b*$^{m-/-}$ and DKO mice as measured by NMR (Figure 5B) or by the weight from individual fat pads (Figure 5D). Fat free mass was significantly increased in the DKO compared to *Cpt1b*$^{m-/-}$ mice (Figure 5C). Gastrocnemius and quadriceps muscles were heavier in both DKO and *Fgf21*$^{-/-}$ mice, but liver, kidney and heart weights were not significantly higher in DKO mice compared to *Cpt1b*$^{m-/-}$ mice (Figure 5D). Body length was significantly decreased in both *Cpt1b*$^{m-/-}$ and DKO mice compared to control mice, whereas *Fgf21*$^{-/-}$ mice appeared to have significantly longer body length than *Cpt1b*$^{m-/-}$ and DKO mice (Figure 5E). *Cpt1b*$^{m-/-}$ mice have reduced activity leading to an overall decrease in energy expenditure (Wicks et al., 2015) (Figure 5F). The decreased activity in *Cpt1b*$^{m-/-}$ mice is almost restored by the lack of FGF21 in the DKO mice with a concomitant increase in energy expenditure (Figure 5F). Additionally, RER in DKO mice was comparable to control mice (Figure 5F).

As we previously reported, inhibition of mitochondrial FAO specifically in skeletal muscle results in favorable metabolic adaptations in muscle such as compensatory increases in carbohydrate oxidation, amino acid oxidation, and peroxisomal fat oxidation. Likewise, we observed increased peroxisomal oxidation of the very long chain fatty acid lignocerate (Figure 5G), enhanced pyruvate dehydrogenase activity and pyruvate oxidation through the TCA cycle (Figure 5H), and leucine oxidation in skeletal muscle homogenates from *Cpt1b*$^{m-/-}$ mice compared to control mice (Figure 5I). Notably, expression of mitochondrial biogenesis genes in muscle of DKO was comparable to the increased level in *Cpt1b*$^{m-/-}$ muscle (Figure S6A). Loss of FGF21 itself had very little effect on oxidation, but the combined loss of CPT1b and FGF21 in the DKO mice further increased pyruvate dehydrogenase activity, increased pyruvate oxidation through the TCA cycle, leucine oxidation and peroxisomal oxidation (Figure 5G–5I). In summary, overall fat mass is not increased in DKO mice. Rather elevated FGF21 in *Cpt1b*$^{m-/-}$ mice seems to regulate muscle mass, activity and energy expenditure in a negative manner.

Glucose utilization and insulin signaling are partially regulated by FGF21 in *Cpt1b*$^{m-/-}$ mice

Blood glucose levels are significantly decreased in *Cpt1b*$^{m-/-}$ mice compared to control (*Cpt1b*$^{fl/fl}$) mice during a Glucose Tolerance Test (GTT), indicating improved glucose clearance. This improvement was partially negated in the DKO mice compared to *Cpt1b*$^{m-/-}$ mice (Figure 6A). Compared to control mice, insulin-stimulated glucose clearance was also improved in *Cpt1b*$^{m-/-}$ mice during an Insulin Tolerance Test (ITT). Similar to the GTT, these improvements in insulin sensitivity were negated in the DKO mice compared to *Cpt1b*$^{m-/-}$ mice (Figure 6B). Consistent with this, basal phosphorylation of Akt (Ser473) in skeletal muscle of DKO mice was significantly higher compared to *Cpt1b*$^{m-/-}$ muscle, whereas it was significantly lower compared to *Fgf21*$^{-/-}$ muscle and was indifferent compared to control mice (Figure 6C). However, insulin-stimulated phosphorylation of Akt (Ser473) in muscle of DKO was comparable to levels in control and *Cpt1b*$^{m-/-}$ muscle (Figure 6D). Phosphorylation of Akt1 (Ser473) at baseline was not different between all genotypes (Figure 6E). However, Akt1 phosphorylation in response to insulin in muscle of DKO mice was similar to *Cpt1b*$^{m-/-}$ muscle and was significantly increased compared to control mice (Figure 6F), indicating again that Fgf21 is downstream of Akt1-signaling in *Cpt1b*-deficient muscle (Figure 2H). Notably, reduced phosphorylation of Akt2 (Ser474) at baseline in skeletal muscle of *Cpt1b*$^{m-/-}$ mice was reversed in muscle from DKO mice to that comparable to control mice (Figure 6G), whereas Akt2 phosphorylation in response to insulin was comparable between all genotypes (Figure 6H). These data reinforce a possible feedback inhibition of mTORC1 by FGF21 through which FGF21 contributes to enhanced basal insulin sensitivity in *Cpt1b*$^{m-/-}$ mice (Figure 2H).

Muscle-derived FGF21 promotes browning of iWAT in *Cpt1b*$^{m-/-}$ mice

Since serum FGF21 levels were significantly higher in both fed and fasted states in *Cpt1b*$^{m-/-}$ mice (Figure 1A), we examined FGF21-signaling in other metabolic tissues in *Cpt1b*$^{m-/-}$ mice. Gene expression of *Klb* and *Fgfr1b* was significantly increased in white adipose tissue (WAT) of *Cpt1b*$^{m-/-}$ mice compared to *Cpt1b*$^{fl/fl}$ mice without changes in *Fgfr1c* expression, which would facilitate enhanced FGF21 signaling in WAT (Figure 7A–

7B and S6B). Consistent with previous reports that FGF21 exerts metabolic action enhancing lipolysis, fat oxidation (Coskun et al., 2008), and accumulation of beige adipocytes in other metabolic tissues (Fisher et al., 2012; Keipert et al., 2014), expression of *Pnpla2, Hadha* and *Cs* genes was significantly upregulated in WAT of *Cpt1b*$^{m-/-}$ mice compared to control mice, without affecting liver expression (Figure 7C–7E and S6C). Collectively, these data are consistent with elevated lipolysis and lipid oxidation in WAT depots, but not in liver of *Cpt1b*$^{m-/-}$ mice (Figure 7C–7E and S6C). This seems to be at least partially mediated via FGF21, as DKO mice exhibit significantly attenuated gene expression of lipolytic marker *Pnpla2* (*Atgl*) in WAT of DKO mice compared to *Cpt1b*$^{m-/-}$ mice (Figure 7C), as well as reduced expression of fat oxidation markers *Hadha* and *Cs* in iWAT of DKO mice (Figure 7D–7E). Alternatively, *Hadha* and *Cs* gene expression was similar in eWAT of DKO mice compared to *Cpt1b*$^{m-/-}$ mice (Figure 7D–7E).

Additionally, expression of brown adipocyte markers such as *Ucp1*and *Cidea* was significantly increased in iWAT, but not in eWAT of *Cpt1b*$^{m-/-}$ mice compared to control mice (Figure 7F and S6D). Notably, expression of *Ucp1* and *Cidea* was entirely attenuated in iWAT of *Fgf21*$^{-/-}$ and DKO mice compared to *Cpt1b*$^{m-/-}$ mice (Figure 7F). Given the reversal of FAO enzymes and *Ucp1* and *Cidea* expression by loss of FGF21 in the DKO mice, increased fat mass might be expected. However, neither fat mass by NMR (Figure 5B), nor individual fat pad weight (Figure 5D) were different between DKO mice and *Cpt1b*$^{m-/-}$ mice. Also there is an obvious decrease in adipocyte size in *Cpt1b*$^{m-/-}$ mice compared to control mice that is not changed by the loss of FGF21 (Figure 7G).

Effects on liver, pancreas, IGF-1 and adiponectin in *Cpt1b*$^{m-/-}$ mice

The pancreas and liver are both known producers and targets of FGF21 (Fon Tacer et al., 2010). In Figure 1B we reported no increase in FGF21 expression in liver of *Cpt1b*$^{m-/-}$ mice. Likewise the expression of *Klb* and *Fgfr4, and Fgfr1c* in liver of *Cpt1b*$^{m-/-}$ mice was unaltered compared to *Cpt1b*$^{fl/fl}$ mice (Figure S6E–S6F). Expression of *Fgfr1b* was significantly increased in liver of *Cpt1b*$^{m-/-}$ mice. However, the expression level was negligible compared to expression of other Fgf-receptors in liver (Figure S6F). In addition, gene expression of *Fgf21* and as well as *Klb* and *Fgf*-receptors in pancreas was comparable between *Cpt1b*$^{m-/-}$ and *Cpt1b*$^{fl/fl}$ mice (Figure S6G–S6H).

In a transgenic animal model, it has been shown that FGF21 overexpressing mice have significantly lower levels of IGF-1 compared to wild-type mice (Inagaki et al., 2008). Of note, serum levels of IGF-1 were significantly lower in *Cpt1b*$^{m-/-}$ mice (*n=52–59*, Figure S7A). In a smaller cohort, IGF-1 was significantly lower in *Cpt1b*$^{m-/-}$ mice and DKO mice compared to control and *Fgf21*$^{-/-}$ mice (Figure S7B). These data are consistent with decreased body length in *Cpt1b*$^{m-/-}$ and DKO mice (Figure 5E), but do not suggest that reduced IGF-1 is driven by increased circulating FGF21 in *Cpt1b*$^{m-/-}$ mice. Though the metabolic effect of FGF21 has been shown to be dependent upon adiponectin (Holland et al., 2013), the expression of adiponectin receptors, *Adipor1* and *Adipor2* was not different in skeletal muscle between *Cpt1b*$^{m-/-}$ and *Cpt1b*$^{fl/fl}$ mice (Figure S6C–S6D). Notably, serum levels of total and high molecular weight adiponectin were also similar between *Cpt1b*$^{m-/-}$ and *Cpt1b*$^{fl/fl}$ mice (Figure S6E–S6F). This is consistent with a recent paper (Kolumam et

al., 2015) demonstrating FGF21mimetic antibody having metabolic effects in adiponectin-KO mice.

DISCUSSION

Previously, we showed that AMPK/PGC1α activated by energy deprivation orchestrates compensatory increases in mitochondrial biogenesis, mitochondrial oxidative capacity, fat oxidation by peroxisomes, and usage of amino acids as energy sources in *Cpt1b*$^{m-/-}$ muscle (Wicks et al., 2015). Here we show that AMPK, through activation of the TSC-complex, 1) activates mTORC2-Akt1-FGF21 leading to an increase in Glut1 and 2) inactivates mTORC1-S6K-IRS-1 serine phosphorylation. Both of which stimulate glucose uptake at low insulin levels.

The induction of FGF21 in response to impaired mitochondrial FAO in skeletal muscle is a part of several compensatory adaptations designed to maintain energy supply to muscle in *Cpt1b*$^{m-/-}$ mice. While liver is considered the major organ for the upregulation and secretion of FGF21 in an energy/nutrient deficient state, muscle has also been shown to secret FGF21. Energy deficit caused by respiratory chain deficiencies leads to mitochondrial myopathy and increased FGF21 production in mice and humans (Suomalainen et al., 2011; Tyynismaa et al., 2010). In another model of mitochondrial inefficiency, muscle specific over expression of UCP-1 causes FGF21 upregulation in skeletal muscle (Keipert et al., 2014; Ost et al., 2016). Dysregulation of lipid delivery to mitochondria by either overexpression of perilipin 5 (Harris et al., 2015) or deletion of the lipase ATGL (Brahma et al., 2014), leads to FGF21 induction in skeletal muscle or heart, respectively. Taken together with our data these results suggest that many pathophysiological conditions (disorders of lipid uptake and transport, lipid droplet formation and lipolysis, any defect in the carnitine shuttle system, disorders of mitochondrial FAO, and mitochondrial dysfunction) will stimulate FGF21 production in muscle.

All of the above models represent rather severe conditions that identified specific pathways for FGF21 regulation in muscle. While still not physiological, one study demonstrated that after a prolonged 3–4 hour hyperinsulinemic/euglycemic clamp, both skeletal muscle FGF21 mRNA and circulating FGF21 were increased (Hojman et al., 2009). The hyperinsulinemic/euglycemic clamp procedure itself can be considered as a period of suppression of FAO. In the present study, we demonstrate that there is minimal FGF21 expression in murine or human primary myotubes and incubation of either murine or human primary myotubes with a palmitate:oleate mixture or the CPT1 inhibitor etomoxir alone has no effect on FGF21 mRNA. However, the combination of fatty acids and etomoxir increases FGF21 expression nearly 10-fold (Figure 3A–C). We also demonstrate that the FGF21 induction is blunted in differentiated myotubes from obese-diabetic subjects. Moreover, we observe decreased mitochondrial FAO induces FGF21 in otherwise “healthy” myotubes. We also demonstrate that the regulation of FGF21 production appears to be mediated through an AMPK-the mTOR-Akt1 axis (Figure 3A–C). This is in agreement with a transgenic mouse model where overexpression of Akt1 induces FGF21 secretion from muscle (Izumiya et al., 2008). Two previous studies report beneficial effects of FGF21 treatment on human myotubes by increasing glucose uptake (Mashili et al., 2011) and suppressing NF-kB (Lee et al., 2012).

We further show that FGF21 has beneficial effects in human myotubes. FGF21 was able to repress mTORC1, leading to subsequent repression of IRS1-phosphorylation at Ser636/639 and improved downstream insulin signaling in the presence of FA.

There are a number of studies demonstrating the induction of FGF21 requires an activating transcription factor 4 (ATF4)-dependent mechanism (De Sousa-Coelho et al., 2012; Kim et al., 2013a; Kim et al., 2013b; Ost et al., 2016; Tyynismaa et al., 2010). We were surprised to see no changes in Aft4 mRNA or protein levels in *Cpt1b*$^{m-/-}$ mice. Additionally, markers for oxidative stress (*Nrf2*), hypoxia (*Hif1α*), ER stress (unspliced *Xbp1u* and spliced *Xbp1s, Ddit3*) were not elevated in *Cpt1b*$^{m-/-}$ muscle (Figure 4). Also, a comprehensive global expression analysis demonstrated that ER stress, Autophagy and Mitophagy pathways are not significantly different between *Cpt1b*$^{m-/-}$ and control mice (Figure S3–S5). In fact, in spite of the accumulation of total lipid and lipotoxic intermediates the skeletal muscle from *Cpt1b*$^{m-/-}$ mice has characteristics similar to trained athletes (Goodpaster et al., 2001) including increased glucose and lipid uptake, large lipid droplets, increased mitochondrial biogenesis, and increased mitochondrial oxidative capacity although *Cpt1b*$^{m-/-}$ mice are hypoactive (Wicks et al., 2015).

When we investigated the role of muscle-derived FGF21 in the obesity-resistant phenotype in *Cpt1b*$^{m-/-}$ mice at the whole body level (see figure 7H for summary), DKO mice showed a modest attenuation in the body weight reduction observed in *Cpt1b*$^{m-/-}$ mice. However, the increase in body weight between *Cpt1b*$^{m-/-}$ and DKO mice was entirely accounted for by an increase in FFM in DKO mice. The decreased fat mass and body length observed in *Cpt1b*$^{m-/-}$ mice was not corrected by the absence of FGF21. Examination of individual tissues again shows that the reduced fat mass in *Cpt1b*$^{m-/-}$ mice is not increased in DKO mice. Likewise, the mass of major organs such as liver, heart and kidney are still reduced in DKO mice. We did observe an increase in skeletal muscle mass in both the *Fgf21*$^{-/-}$ and DKO mice which is probably responsible for the increased FFM. Interestingly, the reduced spontaneous activity observed in *Cpt1b*$^{m-/-}$ mice is normalized in DKO mice. The increased activity may be supported by the increased muscle mass rather than the known effects of FGF21 on torpor and circadian rhythms (Bookout et al., 2013) since activity in the *Fgf21*$^{-/-}$ mice is not above control mice (Figure 5).

The improved glucose uptake during a GTT was partially blunted in the DKO mice and the marginal decrease in blood glucose during an ITT was returned to control levels in DKO mice. At the muscle level, the reduced phosphorylation of Akt2 at baseline in *Cpt1b*$^{m-/-}$ muscle was substantially reversed in muscle of DKO mice, indicating that FGF21 contributes largely to the improvement in basal insulin sensitivity in *Cpt1b*$^{m-/-}$ muscle. When we investigated the role of FGF21 in the increased oxidative capacity of *Cpt1b*$^{m-/-}$ muscle, we found that DKO mice showed further increases in peroxisomal fat oxidation, and carbohydrate and amino acid oxidation. A potential explanation is that beneficial effects of FGF21 on glucose uptake are gone in the DKO and the muscle is further compensating to increase oxidative capacity.

FGF21 has been reported to ameliorate diet-induced obesity and insulin resistance by increasing lipolysis and β-oxidation (Coskun et al., 2008; Inagaki et al., 2007;

Kharitonenkov et al., 2005) We detected elevated markers of mitochondrial number, lipolysis, β-oxidation, and adipocyte browning in WAT of *Cpt1b*$^{m-/-}$ mice. Moreover, expression of browning markers was completely reversed in iWAT of DKO mice reaching levels similar to control mice. However, the reversal of browning markers has no effect on fat mass as measured by NMR, mass of individual fat depots, or adipocyte histology suggesting the level of browning observed in *Cpt1b*$^{m-/-}$ mice is not high enough to increase whole body energy expenditure. The lack of an effect of FGF21 on adiposity was also observed in the transgenic mice overexpressing UCP-1 in skeletal muscle (Ost et al., 2016).

In summary, the combination of elevated fatty acids and CPT1b inhibition increases FGF21 production in skeletal muscle via an AMPK-mTor-Akt1 pathway. Importantly, this regulation does not involve induction of the ER stress pathway which has been reported to be a primary mediator of FGF21 induction in skeletal muscle under pathological conditions. Indeed, results from the present study indicate that production of FGF21 in skeletal muscle of Cpt1bm−/− mice improves metabolic health as FGF21 appears to act in a paracrine manner in muscle to improve glucose uptake in these mice. While circulating FGF21 does produce browning in adipose tissue, FGF21 does not drive the obesity-resistant phenotype observed in *Cpt1b*$^{m-/-}$ mice. As such, further studies are needed to evaluate FGF21-independent pathways in *Cpt1b*$^{m-/-}$ mice that would provide new insights on resistance to diet-induced obesity. Altogether, our findings suggest that pharmacologically targeted CPT1b inhibition specifically in skeletal muscle could trigger favorable adaptive responses resulting in improved glucose uptake and reduced fat mass, and that the improvements in glucose homeostasis are partially driven by muscle-specific upregulation of FGF21.

EXPERIMENTAL PROCEDURES

Animal Studies

Animal studies were conducted at Pennington Biomedical Research Center's AALAC-approved facility on a standard breeder chow diet, composed of 20% protein, 25% fat, 55% carbohydrate (Purina Rodent Chow no. 5015, Purina Mills, St. Louis, MO, USA). All experiments were in compliance with the NIH Guide for the Care and Use of Laboratory Animals, and approved by the Institutional Animal Care and Use Committee. All mice utilized in the experiments were 3–4 month old unless specified otherwise.

Animal Procedures

Serum and plasma collections were performed by submandibular bleed. GTT were performed following a 4-h fast by i.p. injection of 10% D-glucose (0.68 g/kg body weight). ITT were done in the fed state using an i.p. dose of 0.04 u/kg body weight. For insulin signaling studies, mice were fasted overnight, given an intraperitoneal injection of insulin (1.0 U/kg body weight), and tissues were collected 10 minutes later. Indirect calorimetry was done in a 16-chamber Oxymax system (Columbus Instruments) (Wicks et al., 2015).

ELISA

ELISA kits were used for measurement of FGF21 (BioVendor, Asheville, NC, USA) in serum and supernatant of mouse primary muscle cell culture, and IGF-1 (Abcam,

Cambridge, MA, USA) in serum, and total and high molecular weight adiponectin (ALPCO Diagnostics, Salem, NH, USA) in plasma.

Quantitative RT-PCR

qRT-PCR was conducted using $\Delta\Delta C_T$ assay as described previously (Vandanmagsar et al., 2011). Mouse and human cyclophilin B were used as a housekeeping gene control for normalization of gene expression. Primer details are provided in Supplementary Table 1.

Western blot analysis

Protein homogenates were prepared from muscle tissue in Cell Lysis Buffer (EMD Millipore, Danvers, MA, USA). Immunoblot analyses were performed using standard procedures. See Supplementary Methods for details.

Mouse primary muscle cell culture

Cultures were established from mixed hindlimb muscle from 1 month and 3–5 month old *Cpt1b*$^{m-/-}$ and *Cpt1b*$^{fl/fl}$ littermates (Rando and Blau, 1994). See Supplementary Methods for details.

Human skeletal muscle myoblast culture

Cryopreserved human skeletal muscle myoblasts (HSMM) from four Normal-Lean (BMI, 19.8±0.7), and four Diabetic-Obese (BMI, 32.6±4.2) subjects at passage 2 were purchased from Lonza (Walkersville, MD, USA) and cultured as previously described (Vandanmagsar et al., 2014). See Supplementary Methods for details.

Multiplex Mapmate signaling assay

Harvested muscle tissue from mouse was snap froze in liquid nitrogen. Then entire muscle tissue was powdered in liquid nitrogen and used for protein lysate preparation in Cell Signaling Lysis Buffer (Millipore). Differentiated and treated human myotubes were harvested in Cell Signaling Lysis Buffer (Millipore). See Supplementary Methods for details.

Glucose Uptake

Glucose uptake was measured in mouse primary myotubes as described in (Noland et al., 2009). See Supplementary Methods for details.

Substrate Oxidation Assays

Gastrocnemius muscle homogenates were prepared as previously described (Noland et al., 2007). Peroxisomal FAO was measured from [1-^{14}C]lignoceric acid (20 uM), PDH activity and pyruvate oxidation were measured from [1-^{14}C] and [3-^{14}C] puruvate, leucine oxidation was measured by capturing $^{14}CO_2$ from [U-^{14}C]Leu (100 uM) as previously described (Wicks et al., 2015).

Statistical Analysis

Data are expressed as mean ± s.e.m. GraphPad Prism 5 software was used for analysis of variance with ANOVA/repeated measures ANOVA and Bonferroni post-tests or two-tailed Student's *t*-test. $P < 0.05$ was considered significant.

Supplementary Material

Refer to Web version on PubMed Central for supplementary material.

Acknowledgments

This work utilized PBRC core facilities that are supported in part by COBRE (NIH 8 P20-GM103528) and NORC (NIH 2P30-DK072476) center grants from the National Institutes of Health. This research was supported by ADA grant # 1-10-BS-129 and NIH grant R01DK089641 to R.L.M. R.C.N. is supported by R01DK103860. J.D.W is supported by T32 fellowship T32DK6458413. This work was also supported in part by National Institutes of Health (NIH) grant 1U54-GM-104940, which funds the Louisiana Clinical and Translational Science Center.

References

Badman MK, Koester A, Flier JS, Kharitonenkov A, Maratos-Flier E. Fibroblast growth factor 21-deficient mice demonstrate impaired adaptation to ketosis. Endocrinology. 2009; 150:4931–4940. [PubMed: 19819944]

Badman MK, Pissios P, Kennedy AR, Koukos G, Flier JS, Maratos-Flier E. Hepatic fibroblast growth factor 21 is regulated by PPARalpha and is a key mediator of hepatic lipid metabolism in ketotic states. Cell Metab. 2007; 5:426–437. [PubMed: 17550778]

Bookout AL, de Groot MH, Owen BM, Lee S, Gautron L, Lawrence HL, Ding X, Elmquist JK, Takahashi JS, Mangelsdorf DJ, et al. FGF21 regulates metabolism and circadian behavior by acting on the nervous system. Nature medicine. 2013; 19:1147–1152.

Brahma MK, Adam RC, Pollak NM, Jaeger D, Zierler KA, Pocher N, Schreiber R, Romauch M, Moustafa T, Eder S, et al. Fibroblast growth factor 21 is induced upon cardiac stress and alters cardiac lipid homeostasis. J Lipid Res. 2014; 55:2229–2241. [PubMed: 25176985]

Brooks GA. Importance of the 'crossover' concept in exercise metabolism. Clin Exp Pharmacol Physiol. 1997; 24:889–895. [PubMed: 9363377]

Brooks GA, Mercier J. Balance of carbohydrate and lipid utilization during exercise: the "crossover" concept. J Appl Physiol (1985). 1994; 76:2253–2261. [PubMed: 7928844]

Chen WS, Xu PZ, Gottlob K, Chen ML, Sokol K, Shiyanova T, Roninson I, Weng W, Suzuki R, Tobe K, et al. Growth retardation and increased apoptosis in mice with homozygous disruption of the Akt1 gene. Genes Dev. 2001; 15:2203–2208. [PubMed: 11544177]

Chiang GG, Abraham RT. Phosphorylation of mammalian target of rapamycin (mTOR) at Ser-2448 is mediated by p70S6 kinase. J Biol Chem. 2005; 280:25485–25490. [PubMed: 15899889]

Chong-Kopera H, Inoki K, Li Y, Zhu T, Garcia-Gonzalo FR, Rosa JL, Guan KL. TSC1 stabilizes TSC2 by inhibiting the interaction between TSC2 and the HERC1 ubiquitin ligase. J Biol Chem. 2006; 281:8313–8316. [PubMed: 16464865]

Copps KD, White MF. Regulation of insulin sensitivity by serine/threonine phosphorylation of insulin receptor substrate proteins IRS1 and IRS2. Diabetologia. 2012; 55:2565–2582. [PubMed: 22869320]

Coskun T, Bina HA, Schneider MA, Dunbar JD, Hu CC, Chen Y, Moller DE, Kharitonenkov A. Fibroblast growth factor 21 corrects obesity in mice. Endocrinology. 2008; 149:6018–6027. [PubMed: 18687777]

Dagenais GR, Tancredi RG, Zierler KL. Free fatty acid oxidation by forearm muscle at rest, and evidence for an intramuscular lipid pool in the human forearm. J Clin Invest. 1976; 58:421–431. [PubMed: 956375]

De Sousa-Coelho AL, Marrero PF, Haro D. Activating transcription factor 4-dependent induction of FGF21 during amino acid deprivation. Biochem J. 2012; 443:165–171. [PubMed: 22233381]

Ferre P. The biology of peroxisome proliferator-activated receptors: relationship with lipid metabolism and insulin sensitivity. Diabetes. 2004; 53(Suppl 1):S43–50. [PubMed: 14749265]

Fisher FM, Kleiner S, Douris N, Fox EC, Mepani RJ, Verdeguer F, Wu J, Kharitonenkov A, Flier JS, Maratos-Flier E, et al. FGF21 regulates PGC-1alpha and browning of white adipose tissues in adaptive thermogenesis. Genes Dev. 2012; 26:271–281. [PubMed: 22302939]

Fon Tacer K, Bookout AL, Ding X, Kurosu H, John GB, Wang L, Goetz R, Mohammadi M, Kuro-o M, Mangelsdorf DJ, et al. Research resource: Comprehensive expression atlas of the fibroblast growth factor system in adult mouse. Mol Endocrinol. 2010; 24:2050–2064. [PubMed: 20667984]

Garofalo RS, Orena SJ, Rafidi K, Torchia AJ, Stock JL, Hildebrandt AL, Coskran T, Black SC, Brees DJ, Wicks JR, et al. Severe diabetes, age-dependent loss of adipose tissue, and mild growth deficiency in mice lacking Akt2/PKB beta. J Clin Invest. 2003; 112:197–208. [PubMed: 12843127]

Goodpaster BH, He J, Watkins S, Kelley DE. Skeletal muscle lipid content and insulin resistance: evidence for a paradox in endurance-trained athletes. J Clin Endocrinol Metab. 2001; 86:5755–5761. [PubMed: 11739435]

Gorentla BK, Wan CK, Zhong XP. Negative regulation of mTOR activation by diacylglycerol kinases. Blood. 2011; 117:4022–4031. [PubMed: 21310925]

Guridi M, Tintignac LA, Lin S, Kupr B, Castets P, Ruegg MA. Activation of mTORC1 in skeletal muscle regulates whole-body metabolism through FGF21. Sci Signal. 2015; 8:ra113. [PubMed: 26554817]

Harris LA, Skinner JR, Shew TM, Pietka TA, Abumrad NA, Wolins NE. Perilipin 5-Driven Lipid Droplet Accumulation in Skeletal Muscle Stimulates the Expression of Fibroblast Growth Factor 21. Diabetes. 2015; 64:2757–2768. [PubMed: 25829453]

Haynes CM, Ron D. The mitochondrial UPR - protecting organelle protein homeostasis. J Cell Sci. 2010; 123:3849–3855. [PubMed: 21048161]

Hojman P, Pedersen M, Nielsen AR, Krogh-Madsen R, Yfanti C, Akerstrom T, Nielsen S, Pedersen BK. Fibroblast growth factor-21 is induced in human skeletal muscles by hyperinsulinemia. Diabetes. 2009; 58:2797–2801. [PubMed: 19720803]

Holland WL, Adams AC, Brozinick JT, Bui HH, Miyauchi Y, Kusminski CM, Bauer SM, Wade M, Singhal E, Cheng CC, et al. An FGF21-adiponectin-ceramide axis controls energy expenditure and insulin action in mice. Cell Metab. 2013; 17:790–797. [PubMed: 23663742]

Hotta Y, Nakamura H, Konishi M, Murata Y, Takagi H, Matsumura S, Inoue K, Fushiki T, Itoh N. Fibroblast growth factor 21 regulates lipolysis in white adipose tissue but is not required for ketogenesis and triglyceride clearance in liver. Endocrinology. 2009; 150:4625–4633. [PubMed: 19589869]

Huang J, Manning BD. The TSC1-TSC2 complex: a molecular switchboard controlling cell growth. Biochem J. 2008; 412:179–190. [PubMed: 18466115]

Huang J, Manning BD. A complex interplay between Akt, TSC2 and the two mTOR complexes. Biochem Soc Trans. 2009; 37:217–222. [PubMed: 19143635]

Inagaki T, Dutchak P, Zhao G, Ding X, Gautron L, Parameswara V, Li Y, Goetz R, Mohammadi M, Esser V, et al. Endocrine regulation of the fasting response by PPARalpha-mediated induction of fibroblast growth factor 21. Cell Metab. 2007; 5:415–425. [PubMed: 17550777]

Inagaki T, Lin VY, Goetz R, Mohammadi M, Mangelsdorf DJ, Kliewer SA. Inhibition of growth hormone signaling by the fasting-induced hormone FGF21. Cell Metab. 2008; 8:77–83. [PubMed: 18585098]

Inoki K, Zhu T, Guan KL. TSC2 mediates cellular energy response to control cell growth and survival. Cell. 2003; 115:577–590. [PubMed: 14651849]

Izumiya Y, Bina HA, Ouchi N, Akasaki Y, Kharitonenkov A, Walsh K. FGF21 is an Akt-regulated myokine. FEBS Lett. 2008; 582:3805–3810. [PubMed: 18948104]

Keipert S, Ost M, Johann K, Imber F, Jastroch M, van Schothorst EM, Keijer J, Klaus S. Skeletal muscle mitochondrial uncoupling drives endocrine cross-talk through the induction of FGF21 as a

myokine. American journal of physiology Endocrinology and metabolism. 2014; 306:E469–482. [PubMed: 24347058]

Kelley DE, Mokan M, Simoneau JA, Mandarino LJ. Interaction between glucose and free fatty acid metabolism in human skeletal muscle. J Clin Invest. 1993; 92:91–98. [PubMed: 8326021]

Kharitonenkov A, Shiyanova TL, Koester A, Ford AM, Micanovic R, Galbreath EJ, Sandusky GE, Hammond LJ, Moyers JS, Owens RA, et al. FGF-21 as a novel metabolic regulator. J Clin Invest. 2005; 115:1627–1635. [PubMed: 15902306]

Kim DH, Sarbassov DD, Ali SM, King JE, Latek RR, Erdjument-Bromage H, Tempst P, Sabatini DM. mTOR interacts with raptor to form a nutrient-sensitive complex that signals to the cell growth machinery. Cell. 2002; 110:163–175. [PubMed: 12150925]

Kim KH, Jeong YT, Kim SH, Jung HS, Park KS, Lee HY, Lee MS. Metformin-induced inhibition of the mitochondrial respiratory chain increases FGF21 expression via ATF4 activation. Biochem Biophys Res Commun. 2013a; 440:76–81. [PubMed: 24041694]

Kim KH, Jeong YT, Oh H, Kim SH, Cho JM, Kim YN, Kim SS, Kim do H, Hur KY, Kim HK, et al. Autophagy deficiency leads to protection from obesity and insulin resistance by inducing Fgf21 as a mitokine. Nature medicine. 2013b; 19:83–92.

Kolumam G, Chen MZ, Tong R, Zavala-Solorio J, Kates L, van Bruggen N, Ross J, Wyatt SK, Gandham VD, Carano RA, et al. Sustained Brown Fat Stimulation and Insulin Sensitization by a Humanized Bispecific Antibody Agonist for Fibroblast Growth Factor Receptor 1/betaKlotho Complex. EBioMedicine. 2015; 2:730–743. [PubMed: 26288846]

Lee MS, Choi SE, Ha ES, An SY, Kim TH, Han SJ, Kim HJ, Kim DJ, Kang Y, Lee KW. Fibroblast growth factor-21 protects human skeletal muscle myotubes from palmitate-induced insulin resistance by inhibiting stress kinase and NF-kappaB. Metabolism. 2012; 61:1142–1151. [PubMed: 22398021]

Ma L, Chen Z, Erdjument-Bromage H, Tempst P, Pandolfi PP. Phosphorylation and functional inactivation of TSC2 by Erk implications for tuberous sclerosis and cancer pathogenesis. Cell. 2005; 121:179–193. [PubMed: 15851026]

Mashili FL, Austin RL, Deshmukh AS, Fritz T, Caidahl K, Bergdahl K, Zierath JR, Chibalin AV, Moller DE, Kharitonenkov A, et al. Direct effects of FGF21 on glucose uptake in human skeletal muscle: implications for type 2 diabetes and obesity. Diabetes Metab Res Rev. 2011; 27:286–297. [PubMed: 21309058]

Nabben M, Hoeks J, Moonen-Kornips E, van Beurden D, Briede JJ, Hesselink MK, Glatz JF, Schrauwen P. Significance of uncoupling protein 3 in mitochondrial function upon mid- and long-term dietary high-fat exposure. FEBS Lett. 2011; 585:4010–4017. [PubMed: 22115550]

Nishimura T, Nakatake Y, Konishi M, Itoh N. Identification of a novel FGF, FGF-21, preferentially expressed in the liver. Biochim Biophys Acta. 2000; 1492:203–206. [PubMed: 10858549]

Noland RC, Koves TR, Seiler SE, Lum H, Lust RM, Ilkayeva O, Stevens RD, Hegardt FG, Muoio DM. Carnitine insufficiency caused by aging and overnutrition compromises mitochondrial performance and metabolic control. J Biol Chem. 2009; 284:22840–22852. [PubMed: 19553674]

Noland RC, Woodlief TL, Whitfield BR, Manning SM, Evans JR, Dudek RW, Lust RM, Cortright RN. Peroxisomal-mitochondrial oxidation in a rodent model of obesity-associated insulin resistance. American journal of physiology Endocrinology and metabolism. 2007; 293:E986–E1001. [PubMed: 17638705]

Ogawa Y, Kurosu H, Yamamoto M, Nandi A, Rosenblatt KP, Goetz R, Eliseenkova AV, Mohammadi M, Kuro-o M. BetaKlotho is required for metabolic activity of fibroblast growth factor 21. Proc Natl Acad Sci U S A. 2007; 104:7432–7437. [PubMed: 17452648]

Ost M, Coleman V, Voigt A, van Schothorst EM, Keipert S, van der Stelt I, Ringel S, Graja A, Ambrosi T, Kipp AP, et al. Muscle mitochondrial stress adaptation operates independently of endogenous FGF21 action. Mol Metab. 2016; 5:79–90. [PubMed: 26909316]

Rando TA, Blau HM. Primary mouse myoblast purification, characterization, and transplantation for cell-mediated gene therapy. J Cell Biol. 1994; 125:1275–1287. [PubMed: 8207057]

Suomalainen A, Elo JM, Pietilainen KH, Hakonen AH, Sevastianova K, Korpela M, Isohanni P, Marjavaara SK, Tyni T, Kiuru-Enari S, et al. FGF-21 as a biomarker for muscle-manifesting

mitochondrial respiratory chain deficiencies: a diagnostic study. Lancet neurology. 2011; 10:806–818. [PubMed: 21820356]

Tyynismaa H, Carroll CJ, Raimundo N, Ahola-Erkkila S, Wenz T, Ruhanen H, Guse K, Hemminki A, Peltola-Mjosund KE, Tulkki V, et al. Mitochondrial myopathy induces a starvation-like response. Human molecular genetics. 2010; 19:3948–3958. [PubMed: 20656789]

Um SH, Frigerio F, Watanabe M, Picard F, Joaquin M, Sticker M, Fumagalli S, Allegrini PR, Kozma SC, Auwerx J, et al. Absence of S6K1 protects against age- and diet-induced obesity while enhancing insulin sensitivity. Nature. 2004; 431:200–205. [PubMed: 15306821]

Vandanmagsar B, Haynie KR, Wicks SE, Bermudez EM, Mendoza TM, Ribnicky D, Cefalu WT, Mynatt RL. Artemisia dracunculus L. extract ameliorates insulin sensitivity by attenuating inflammatory signalling in human skeletal muscle culture. Diabetes Obes Metab. 2014; 16:728–738. [PubMed: 24521217]

Vandanmagsar B, Youm YH, Ravussin A, Galgani JE, Stadler K, Mynatt RL, Ravussin E, Stephens JM, Dixit VD. The NLRP3 inflammasome instigates obesity-induced inflammation and insulin resistance. Nature medicine. 2011; 17:179–188.

Wicks SE, Vandanmagsar B, Haynie KR, Fuller SE, Warfel JD, Stephens JM, Wang M, Han X, Zhang J, Noland RC, et al. Impaired mitochondrial fat oxidation induces adaptive remodeling of muscle metabolism. Proc Natl Acad Sci U S A. 2015

Wouters BG, Koritzinsky M. Hypoxia signalling through mTOR and the unfolded protein response in cancer. Nat Rev Cancer. 2008; 8:851–864. [PubMed: 18846101]

Wullschleger S, Loewith R, Hall MN. TOR signaling in growth and metabolism. Cell. 2006; 124:471–484. [PubMed: 16469695]

Xu H, Hertzel AV, Steen KA, Wang Q, Suttles J, Bernlohr DA. Uncoupling Lipid Metabolism from Inflammation Through FABP-dependent Expression of UCP2. Mol Cell Biol. 2015

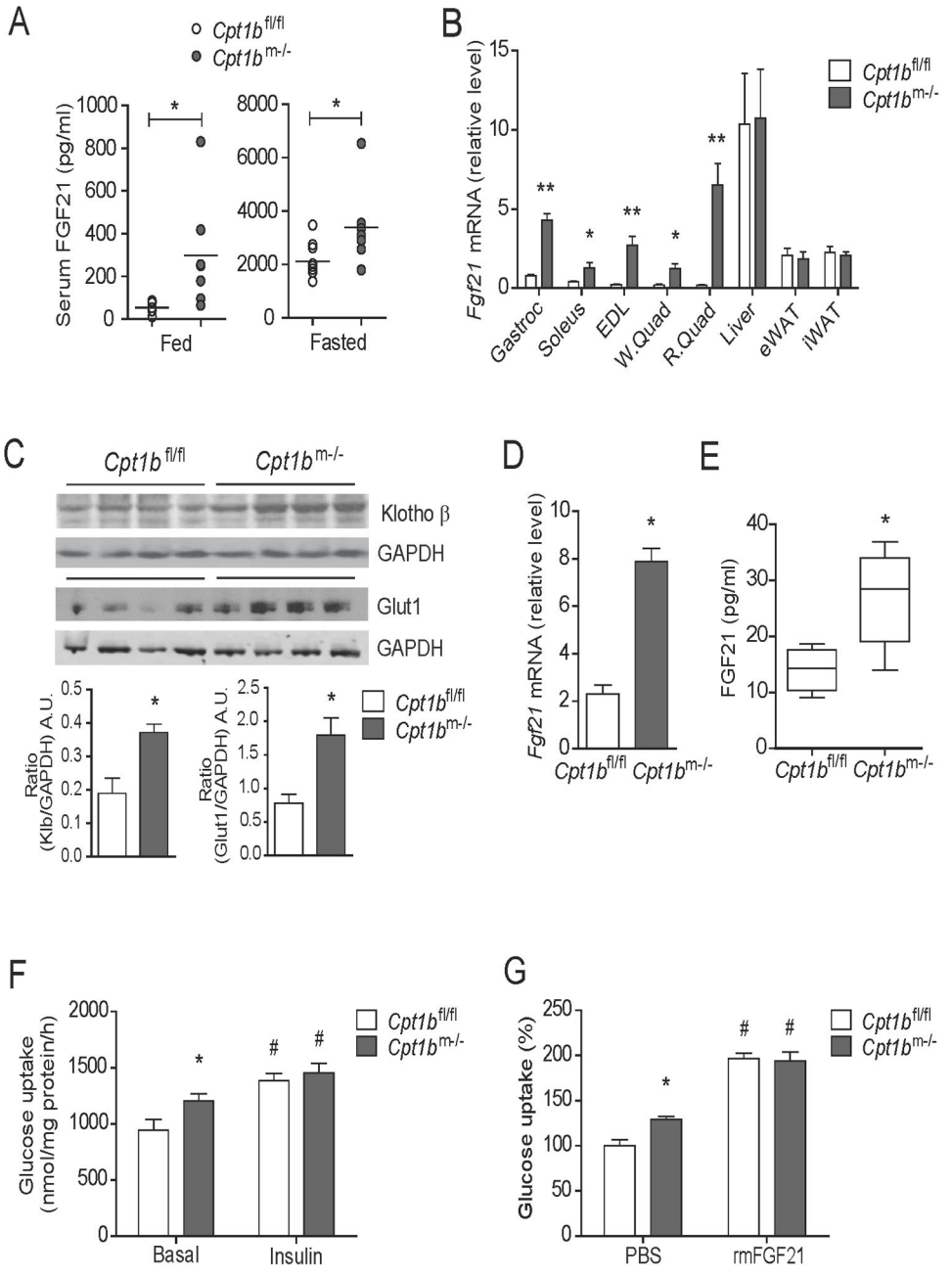

Figure 1. Muscle-derived FGF21 enhances glucose uptake in skeletal muscle in *Cpt1b*$^{m-/-}$ mice

(A) Serum FGF21 concentration in 4 month old *Cpt1b*$^{m-/-}$ and *Cpt1b*$^{fl/fl}$ mice fed and fasted overnight (*n=7–9* per group). (B) *Fgf21* gene expression in muscle tissue such as gastrocnemius (Gastroc), soleus, extensor digitorium longus (EDL), white and red quads (W.Quad and R.Quad), and other tissue such as liver, epididymal and inguinal white adipose tissue (eWAT and iWAT) from 3–5 month old *Cpt1b*$^{m-/-}$ and *Cpt1b*$^{fl/fl}$ mice (*n=5–8*). (C) Immunoblot analysis showing Klotho β and Glut1 protein abundance in gastrocnemius muscle from 4 month old *Cpt1b*$^{m-/-}$ and *Cpt1b*$^{fl/fl}$ mice. GAPDH used as a loading control. Image J software was used for densitometry quantification of the immunoblots. Results shown are representative of three separate experiments (*n=3–4* per group). (D) *Fgf21* gene

expression primary myotubes established from *Cpt1b*$^{m-/-}$ and *Cpt1b*$^{fl/fl}$ mice. (E) Secreted FGF21 over 24h in culture media from primary myotubes initiated from *Cpt1b*$^{m-/-}$ and *Cpt1b*$^{fl/fl}$ mice. (F) Basal and insulin-stimulated [^{3}H]-2-deoxyglucose uptake in primary myotubes from *Cpt1b*$^{m-/-}$ and *Cpt1b*$^{fl/fl}$ mice. (G) Primary myotubes from *Cpt1b*$^{m-/-}$ and *Cpt1b*$^{fl/fl}$ mice (3–5 months of age) were pre-treated with vehicle (PBS) or rmFGF21 (250 ng/ml, 16h) and then [^{3}H]-2-deoxyglucose uptake was measured. Results shown are representative of four independent experiments. All data are presented as means ± s.e.m., $*P < 0.05$ and **P < 0.01 between *Cpt1b*$^{m-/-}$ and *Cpt1b*$^{fl/fl}$ mice, and $^{\#}P < 0.05$ between vehicle versus insulin or rmFGF21 treatments.

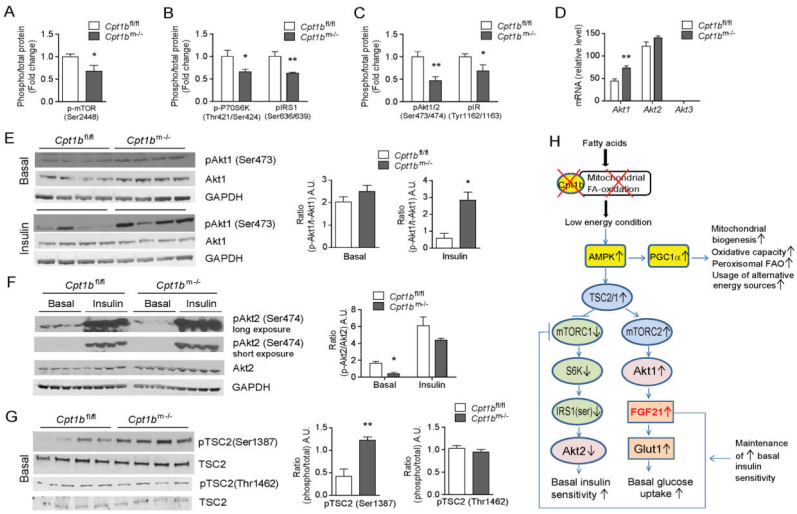

Figure 2. mTOR-Akt signaling pathways are involved in induction of *Fgf21* in energy deficient condition caused by impaired mitochondrial fatty acid oxidation (FAO)

(A–B) Activity of mTOR (A) and downstream members of mTORC1-signaling pathway, P70S6K and IRS1 (B) in gastrocnemius muscle from *Cpt1b*$^{m-/-}$ and *Cpt1b*$^{fl/fl}$ mice. (C) Akt, insulin receptor (IR) signaling at baseline in gastrocnemius muscle from *Cpt1b*$^{m-/-}$ and *Cpt1b*$^{fl/fl}$ mice. (D) Gene expression of Akt-signaling members, *Akt1*, *Akt2* and *Akt3* in gastrocnemius muscle from *Cpt1b*$^{m-/-}$ and *Cpt1b*$^{fl/fl}$ mice (*n=8*). (E–F) Immunoblot analysis of basal and insulin-stimulated Akt1 (E) and Akt2 (F) signaling by phosphorylation at Ser473 and Ser 474, respectively, in red quad muscle from *Cpt1b*$^{m-/-}$ and *Cpt1b*$^{fl/fl}$ mice. GAPDH was used as a loading control. Image J software was used for densitometry quantification of the immunoblots. (G) Activation of TSC2, as examined by phosphorylation at Ser1387 and Thr1462 in red quad muscle from *Cpt1b*$^{m-/-}$ and *Cpt1b*$^{fl/fl}$ mice. Results shown are representative of three independent experiments (*n=4* per group). (H) Proposed model explaining mechanisms of interplay of the AMPK, mTOR, Akt signaling pathways in the FGF21 induction and enhanced glucose utilization in the condition with mitochondrial FAO deficiency. All data are presented as means ± s.e.m., $*P < 0.05$, $**P < 0.01$.

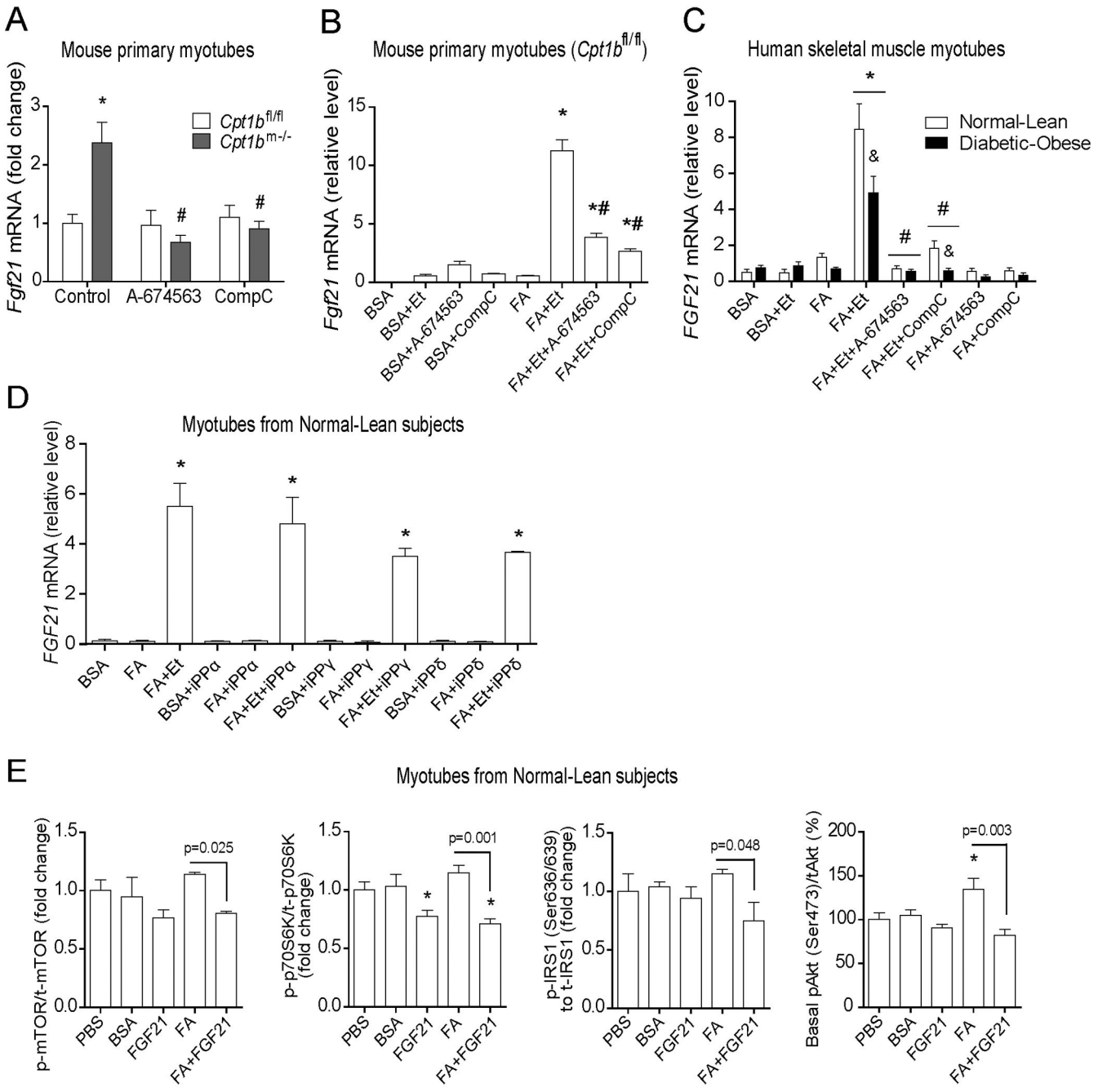

Figure 3. Fgf21 induction in skeletal muscle of *Cpt1b*$^{m-/-}$ mice is AMPK- and Akt1-dependent

(A–B) Gene expression of *Fgf21* in mouse primary myotubes treated with an Akt1 inhibitor, A-674563 (30μM) and an AMPK inhibitor, Compound C (CompC, 30μM) for 24h. (A) Results shown are representative of three independent cultures. *$P < 0.05$ between *Cpt1b*$^{m-/-}$ and *Cpt1b*$^{fl/fl}$ mice, and $^{\#}P < 0.05$ between treatments with vehicle versus inhibitors. (B) Primary muscle cells from *Cpt1b*$^{fl/fl}$ mice. Myotubes were treated with BSA-conjugated FA (0.5 mM) in presence of the Cpt1 inhibitor Etomoxir (Et, 100μM) for 24h. Results shown are representative of 3–4 separate experiments*$P < 0.05$ between control

(BSA) versus other treatments, and $^{\#}P < 0.05$ due to Akt1 or AMPK inhibitors. (C) Gene expression of *FGF21* in human myotubes treated with BSA-conjugated FA (0.5mM) and inhibitors: Etomoxir (Et, 100μM), A-674563 (50μM), and Compound C (CompC, 30μM) for 24h. Human skeletal muscle myoblasts (HSMM) derived from non-diabetic-lean (Normal-Lean) and diabetic-obese subjects were differentiated into myotubes prior to treatments ($n=4$ per group). Results shown are representative of two independent cultures of HSMM per subject. $^{*}P < 0.05$ between treatments with BSA-conjugated FA (FA) versus inhibitors, and $^{\#}P < 0.05$ due to Akt1 or AMPK inhibitors, and $^{\&}P < 0.05$ between myotubes from normal-lean and diabetic-obese subjects. (D) Gene expression of *FGF21* in human myotubes treated with BSA-conjugated FA (0.5mM) and Etomoxir (Et, 100μM) and PPAR-inhibitors: GW6471 (for PPARα, 10μM), T0070907 (for PPARγ, 10μM) and GSK3787 (for PPARδ, 10μM) for 24h. $^{*}P < 0.05$ between treatments with inhibitors versus BSA-control. (E) Activity of mTORC1 and its downstream signaling members P70S6K, IRS1, and basal Akt, as determined by phosphorylation in human myotubes. HSMM originated from normal-lean subjects were differentiated into myotubes prior to treatment with BSA-conjugated FA (0.5mM) and rhFGF21 (200 ng/ml). $^{*}P < 0.05$ between vehicle (PBS) versus other treatments. All data are presented as means ± s.e.m.,

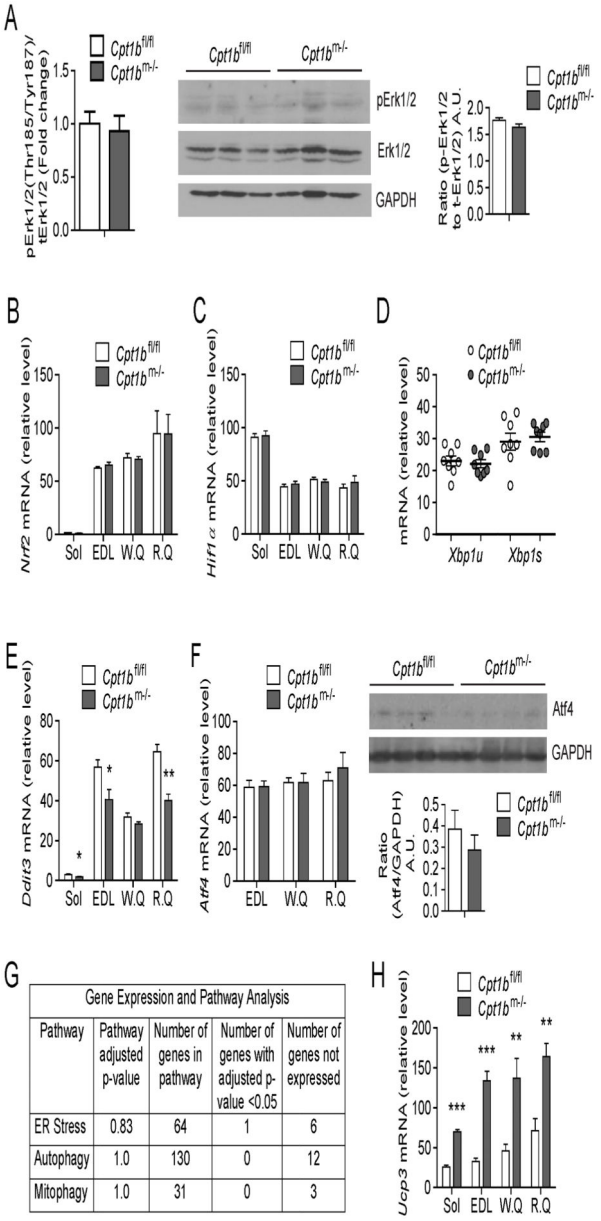

Gene Expression and Pathway Analysis				
Pathway	Pathway adjusted p-value	Number of genes in pathway	Number of genes with adjusted p-value <0.05	Number of genes not expressed
ER Stress	0.83	64	1	6
Autophagy	1.0	130	0	12
Mitophagy	1.0	31	0	3

Figure 4. Stress signaling pathways that are not activated by mitochondrial fat oxidation deficiency

(A) Activity of Erk1/2 signaling pathway, as determined by multiplex protein signaling assay (left) and western blot analysis (center) for phosphorylation in gastrocnemius muscle from 4 month old *Cpt1b*$^{m-/-}$ and *Cpt1b*$^{fl/fl}$ mice (*n=3–4* per group). The Thr185/Tyr187 antibody detects phosphorylation at Thr185 and Tyr187. GAPDH, a loading control. Image J software was used for densitometry quantification of the immunoblots (right). (B–C) Gene expression of oxidative stress (B) and hypoxia (C) markers, as examined by qRT-PCR in muscle. (D–E) Endoplasmic reticulum (ER) stress markers in muscle: Gene expression of unspliced and spliced *Xbp1*(D) and *Ddit3* (E) as determined by qRT-PCR in muscle tissue. Gene expression of uncoupled protein 3 (*Ucp3*), as evaluated by qRT-PCR in skeletal muscle. (F) Gene and protein expression of Atf4, as detected by qRT-PCR and western blot

respectively in skeletal muscle. (G) Summary of results from Gene expression and Pathway analysis for ER stress, autophagy and mitophagy using Gene Ontology and Pathway enrichment analysis on SAGE (Serial Analysis of Gene Expression) data obtained from gastrocnemius muscle. (H) Gene expression of uncoupled protein 3 (*Ucp3*), as evaluated by qRT-PCR in skeletal muscle. Gene expression analysis was performed in muscle tissue such as soleus (Sol), extensor digitorium longus (EDL), white and red quads (W.Q and R.Q) and gastrocnemius from 4 month old $Cpt1b^{m-/-}$ and $Cpt1b^{fl/fl}$ mice (*n=6–8* per group). Immunoblot analysis was performed in gastrocnemius muscle from 4 month old $Cpt1b^{m-/-}$ and $Cpt1b^{fl/fl}$ mice, results shown are representative of three independent experiments (*n=4–6* per group). All data are presented as means ± s.e.m., $*P < 0.05$, $**P < 0.01$, $***P < 0.005$ and higher significance.

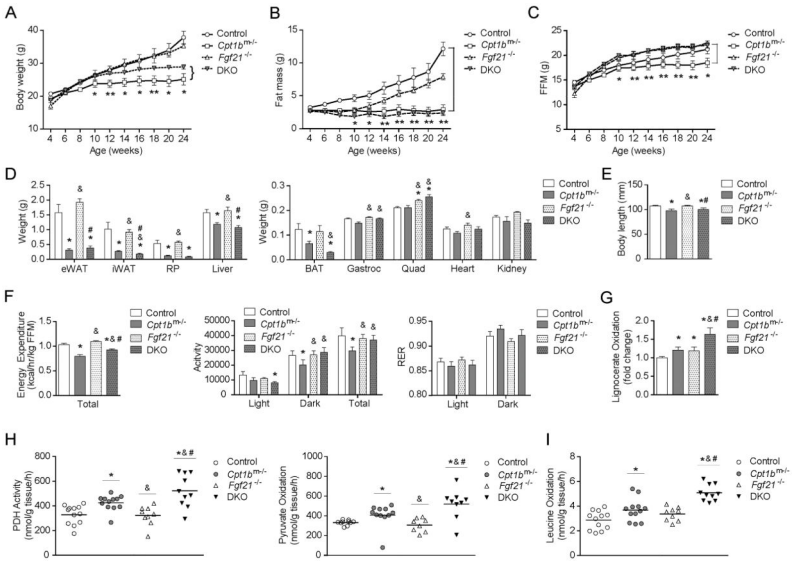

Figure 5. Loss of FGF21 increases muscle mass, activity, energy expenditure and oxidative capacity but does not alter adiposity in *Cpt1b*$^{m-/-}$ mice

(A–C) Body weight (A), fat mass (B) and fat-free mass (FFM; C). *$P < 0.05$ significance when *Cpt1b*$^{m-/-}$ mice were compared to control and DKO mice ($n=7$ per group). (D) Tissue weights ($n=7$). (E) Body length ($n=8–14$). (F) Energy expenditure, activity level and respiratory exchange ratio (RER) ($n=4–6$ per group). (G–I) Substrate oxidation measured in gastrocnemius muscle homogenate from control (*Fgf21*$^{+/+}$ *Cpt1b*$^{fl/fl}$), *Cpt1b*$^{m-/-}$ (*Fgf21*$^{+/+}$ *Cpt1b*$^{m-/-}$), *Fgf21*$^{-/-}$ (*Fgf21*$^{-/-}$ *Cpt1b*$^{fl/fl}$) and DKO (*Fgf21*$^{-/-}$ *Cpt1b*$^{m-/-}$) mice: (G) peroxisomal fatty acid oxidation measured from [1-^{14}C]lignoceric acid (20 uM), (H) Pyruvate dehydrogenase (PDH) activity assayed with [1-^{14}C]pyruvate and pyruvate oxidation measured with [3-^{14}C]pyruvate, (I) leucine oxidation measured from [U-^{14}C]leucine (100 μM). All data are presented as means ± s.e.m., ($n=8–12$ per group), *$P < 0.05$ significance compared to control mice, $^{\&}P < 0.05$ significance compared to *Cpt1b*$^{m-/-}$ mice and $^{\#}P < 0.05$ significance compared to *Fgf21*$^{-/-}$ mice.

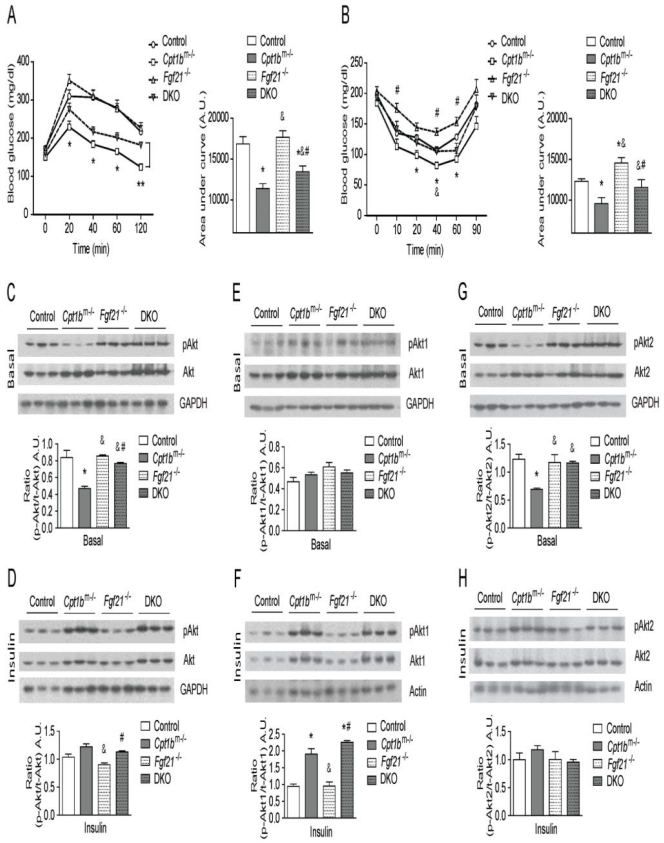

Figure 6. FGF21 is responsible for increased glucose utilization in *Cpt1b*$^{m-/-}$ muscle

(A) GTT (*n=14–22* per group)and (B) ITT (*n=7–11* per group), $^{*}P < 0.05$ significance between control and *Cpt1b*$^{m-/-}$ mice, $^{\#}P < 0.05$ significance between *Cpt1b*$^{m-/-}$ and *Fgf21*$^{-/-}$ mice and $^{\&}P < 0.05$ significance between *Cpt1b*$^{m-/-}$ and DKO mice. (C–H) Immunoblot analysis of Akt-proteins. (C) Basal and (D) Insulin-stimulated phosphorylation of total-Akt at Ser473. (E) Basal and (F) Insulin-stimulated phosphorylation of Akt1 at Ser473. (G) Basal and (H) Insulin-stimulated phosphorylation of Akt2 at Ser474. GAPDH was used as a loading control. Results shown are representative of three independent experiments. Gastrocnemius muscle from control (*Fgf21*$^{+/+}$ *Cpt1b*$^{fl/fl}$), *Cpt1b*$^{m-/-}$ (*Fgf21*$^{+/+}$ *Cpt1b*$^{m-/-}$), *Fgf21*$^{-/-}$ (*Fgf21*$^{-/-}$ *Cpt1b*$^{fl/fl}$) and DKO (*Fgf21*$^{-/-}$ *Cpt1b*$^{m-/-}$) mice were used for all immunoblot analyses (*n=3–5* per group). Image J software was used for densitometry quantification of the immunoblots. All data are presented as means ± s.e.m., $^{*}P < 0.05$ significance compared to control mice, $^{\&}P < 0.05$ significance compared to *Cpt1b*$^{m-/-}$ mice and $^{\#}P < 0.05$ significance compared to *Fgf21*$^{-/-}$ mice.

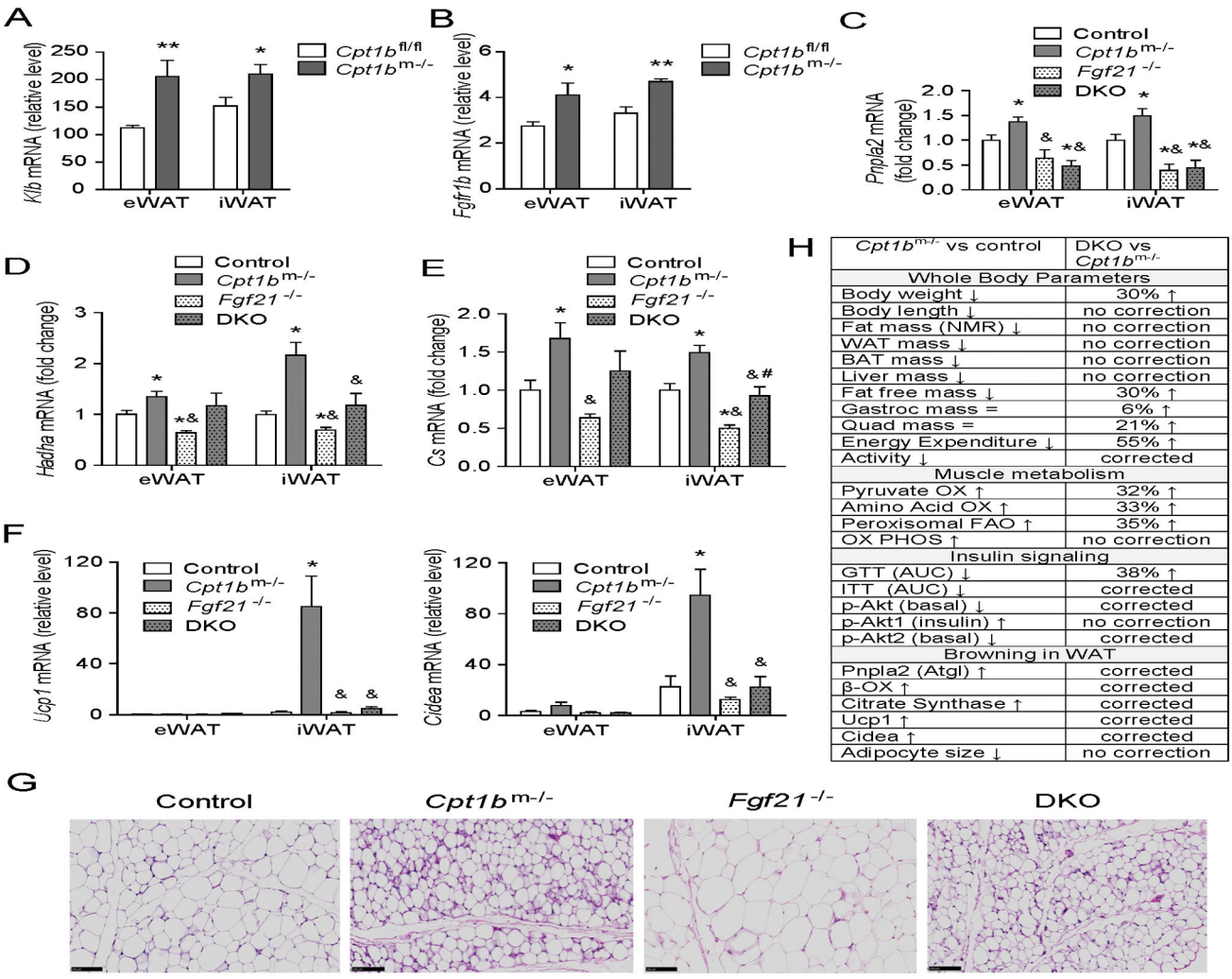

H

Cpt1b m-/- vs control	DKO vs Cpt1b m-/-
Whole Body Parameters	
Body weight ↓	30% ↑
Body length ↓	no correction
Fat mass (NMR) ↓	no correction
WAT mass ↓	no correction
BAT mass ↓	no correction
Liver mass ↓	no correction
Fat free mass ↓	30% ↑
Gastroc mass =	6% ↑
Quad mass =	21% ↑
Energy Expenditure ↓	55% ↑
Activity ↓	corrected
Muscle metabolism	
Pyruvate OX ↑	32% ↑
Amino Acid OX ↑	33% ↑
Peroxisomal FAO ↑	35% ↑
OX PHOS ↑	no correction
Insulin signaling	
GTT (AUC) ↓	38% ↑
ITT (AUC) ↓	corrected
p-Akt (basal) ↓	corrected
p-Akt1 (insulin) ↑	no correction
p-Akt2 (basal) ↓	corrected
Browning in WAT	
Pnpla2 (Atgl) ↑	corrected
β-OX ↑	corrected
Citrate Synthase ↑	corrected
Ucp1 ↑	corrected
Cidea ↑	corrected
Adipocyte size ↓	no correction

Figure 7. Muscle-derived FGF21 enhances browning in white adipose tissue in *Cpt1b*$^{m-/-}$ mice

(A–B) Gene expression of *Klb* (A) and *Fgfr1b* (B) in epididymal and inguinal white adipose tissue (eWAT and iWAT) (*n=5–7* per group). All data are presented as means ± s.e.m., $*P < 0.05$, $**P < 0.005$ and higher significance. (C–E) qRT-PCR analysis of Expression of a lipolytic gene (*Pnpla2*) (C), mitochondrial FAO genes (*Hadha*, *Cs*) (D–E), and beige adipocyte marker genes (*Ucp1, Cidea*) in WAT (F). (G) H&E staining of iWAT. Scale bar indicates 100 μm. (H) Summary of phenotype in *Cpt1b*$^{m-/-}$ mice compared to control mice and the reverse phenotype in DKO mice. Tissue from control (*Fgf21*$^{+/+}$ *Cpt1b*$^{fl/fl}$), *Cpt1b*$^{m-/-}$ (*Fgf21*$^{+/+}$ *Cpt1b*$^{m-/-}$), *Fgf21*$^{-/-}$ (*Fgf21*$^{-/-}$ *Cpt1b*$^{fl/fl}$) and DKO (*Fgf21*$^{-/-}$ *Cpt1b*$^{m-/-}$) mice were used for all qRT-PCR analysis (*n=5–7* per group). All data are presented as means ± s.e.m., $*P < 0.05$ significance compared to control mice, $^{\&}P < 0.05$ significance compared to *Cpt1b*$^{m-/-}$ mice and $^{\#}P < 0.05$ significance compared to *Fgf21*$^{-/-}$ mice.